Conference on Modelling Fluid Flow (CMFF'22)
The 18th International Conference on Fluid Flow Technologies
Budapest, Hungary, August 30-September 2, 2022

A WALL MODEL FOR HIGH-FIDELITY LARGE-EDDY SIMULATION

Lukas UNGLEHRT[1], Johannes KREUZINGER[2], Michael MANHART[3]

[1] Professorship of Hydromechanics, TUM School of Engineering and Design, Technical University of Munich. Arcisstr. 21, 80333 München, Germany. Tel.: +49 289 28565. E-mail: lukas.unglehrt@tum.de
[2] Kreuzinger und Manhart Turbulenz GmbH. E-mail: j.kreuzinger@km-turbulenz.de
[3] Professorship of Hydromechanics, TUM School of Engineering and Design, Technical University of Munich. E-mail: michael.manhart@tum.de

ABSTRACT

We present a novel wall model for well resolved large-eddy simulation (LES) of complex flows. The model is based on a Taylor series expansion of the velocity and pressure profiles in wall-normal direction. The derivatives are determined from the near-wall asymptotics of the Navier-Stokes equations. We take a cubic polynomial for the velocity profile and a linear function for the pressure profile and impose a collocation constraint at a fluid point normal to the wall. This results in an evolution equation for the wall shear stress.

The accuracy of the wall model is assessed with both an a-priori and an a-posteriori approach for the oscillatory Stokes boundary layer and a Falkner-Skan boundary layer. Finally, we apply the model for a LES of turbulent channel flow.

Keywords: boundary layer equations, large eddy simulation, direct numerical simulation, wall model

NOMENCLATURE

U	$[m/s]$	velocity outside the boundary layer
$\Delta x, \Delta y, \Delta z$	$[m]$	cell size
$a, \tilde{a}$	$[1/s]$	velocity gradient
f	$[-]$	stream function
h	$[m]$	channel half-height
p	$[Pa]$	pressure
u, w	$[m/s]$	wall-parallel velocity components
u_τ	$[-]$	friction velocity
v	$[m/s]$	wall-normal velocity component
x, z	$[m]$	wall-parallel coordinates
y	$[m]$	wall-normal coordinate
$\Delta x^+, \Delta y^+, \Delta z^+$	$[-]$	cell size in wall units
$\underline{n}$	$[-]$	wall-normal unit vector
$\underline{u}$	$[m/s]$	velocity vector
$\underline{\underline{I}}$	$[-]$	identity matrix
β	$[-]$	Falkner-Skan parameter
δ_s	$[m]$	Stokes boundary layer thickness $\sqrt{2\nu/\Omega}$
η	$[-]$	dimensionless wall-normal coordinate
η_s	$[-]$	dimensionless wall-normal coordinate
μ	$[Pa \cdot s]$	dynamic viscosity
ν	$[m^2/s]$	kinematic viscosity
Ω	$[1/s]$	frequency
ρ	$[kg/m^3]$	density
$\underline{\tau}_w$	$[Pa]$	wall shear stress vector

Subscripts and Superscripts

$+$	in wall units, i.e. normalised with ν and u_τ
0	amplitude of an oscillation
p	at an interpolation point close to the wall
w	at the wall ($y = 0$)

1. INTRODUCTION

In the simulation of turbulent flow, there exist three principal simulation paradigms. The Reynolds-averaged Navier-Stokes (RANS) equations supplemented with a suitable turbulence model for the Reynolds stresses can be used to approximately compute the time-average velocity field and higher order statistics like the turbulent kinetic energy. The large-eddy simulation (LES) approach explicitly resolves the large, energetic turbulent scales of motion on the numerical grid and only models the stresses arising from the unresolved motion (sub-grid scale or SGS stresses). While the LES comes at a higher computational expense, it is generally considered more reliable for complex flow configurations. The direct numerical simulation resolves all turbulent length and time scales and does not require a turbulent or SGS model. Its accuracy and reliability comes with very large computational costs which inhibits its application at high Reynolds numbers.

In wall-bounded turbulent flow and in flow around bluff bodies, a high grid resolution is necessary in all three simulation paradigms to resolve thin laminar boundary layers or the viscous sublayer of turbulent boundary layers. The wall shear stress

is determined by this viscosity-dominated near wall flow and its accurate prediction is necessary to obtain quantitatively correct results or, e.g. when smooth flow separations are present, even a qualitatively correct flow topology.

In LES, two approaches have been developed to address this problem: wall modeled LES and wall-resolved LES. In wall modeled LES, the wall shear stress is either computed via an assumed velocity profile ("wall function") or by solving a dedicated differential equation on the wall. The former approach commonly relies on the logarithmic velocity profile of turbulent boundary layers or extensions thereof [1]. In the latter approach, some authors solve Reynolds-averaged Navier-Stokes (RANS) equations with a turbulence model on a zonally embedded refined grid near the wall [2, 3]. The velocity boundary conditions for the RANS equations are supplied by the LES and in turn the wall shear stress for the LES results from the RANS solution. In a similar spirit, a wide variety of hybrid RANS/LES models have been developed in which the length-scale of the RANS turbulence model is chosen depending on the grid. The resulting modeled stresses are a mixture between Reynolds stresses and SGS stresses. An example for this is the so-called Detached Eddy Simulation [4]. In wall-resolved LES, the wall shear stress is computed by applying a finite difference approximation. Therefore, high resolutions of approximately one wall unit are required near the wall. The advantage of this approach is that the modeling error is limited to the sub-grid scale model. An intermediate approach between the two paradigms can be realised by blending the wall function with a linear approximation of the velocity profile. For example, the Werner-Wengle wall function [5] uses a linear approximation of the velocity profile if the wall-nearest grid point is below 12 wall units and a $\frac{1}{7}$-th power law at larger wall distances. Based on the grid resolution near the wall, this model results in a wall modeled or a wall-resolved LES. Breuer et al. [6] have extended this model by incorporating pressure gradient effects.

In complex flow configurations where laminar boundary layers, transition to turbulence or flow separation and reattachment may occur, wall functions and RANS-based models have a large uncertainty as the underlying model assumptions – e.g. the presence of a turbulent equilibrium boundary layer – do not always hold in the flow [7, 8]. On the other hand, wall-resolved LES of high-Reynolds number flow can have a prohibitive computational cost, e.g. [9].

In this contribution, we present a wall model for LES that is derived directly from the Navier-Stokes equations under the boundary layer assumptions. The aim of this model is to provide an accurate approximation to the wall shear stress using only information that is available in the wall-nearest cell. In a high-fidelity wall-resolved LES, this allows to choose a coarser grid resolution near the wall while maintaining the predictive quality in complex flow configurations.

2. DERIVATION OF THE WALL MODEL

In this section, we demonstrate how our wall model can be derived. In the first step, the velocity and pressure gradient profiles are approximated by a Taylor series in the wall-normal coordinate.

In the second step (see Sec. 2.1), we determine relations among the expansion coefficients by inserting the expansions into the incompressible Navier-Stokes equations with no-slip conditions. For two-dimensional flow, Dallmann and Gebing [10] have derived such relations from the Taylor series of the streamfunction. Moreover, they recognised that within the region of convergence of the Taylor series of the streamfunction, the velocity field is completely determined by the wall shear stress, the wall pressure and the initial conditions. Consequently, all derivatives occurring in the expansion can be expressed in terms of the wall shear stress and the wall pressure. Also based on the work of [10], Shrikhande [11] investigated the possibility of reconstructing the velocity field from wall shear stress and wall pressure data. They demonstrated their method for various canonical flows and simulations of idealised aircraft wake vortices. They found that the Taylor series converges fast close to the wall and slowly far from the wall. In the present work, we consider the inverse problem – reconstructing the wall shear stress from a known velocity and pressure gradient. We also apply the above derivation to the boundary layer equations to obtain a simplified form of the wall model (see Sec. 2.2).

In the third step (see Sec. 2.3), we truncate the polynomial expansions and impose a collocation condition at a fluid point off the wall. This results in a system of partial differential equations for the wall shear stress with a source term which is a function of quantities at the collocation point. Finally, we discuss the properties of the wall model and possible generalisations (see Sec. 2.4).

2.1. Compatibility conditions from the Navier-Stokes equations

First, the velocity profile is expanded into a Taylor series in the wall distance y:

$$u = u_\mathrm{w} + \left.\frac{\partial u}{\partial y}\right|_\mathrm{w} y + \left.\frac{\partial^2 u}{\partial y^2}\right|_\mathrm{w} \frac{y^2}{2} + \left.\frac{\partial^3 u}{\partial y^3}\right|_\mathrm{w} \frac{y^3}{6} + O(y^4) \quad (1)$$

From the definition of the wall shear stress, the first derivative can be identified as

$$\left.\frac{\partial u}{\partial y}\right|_\mathrm{w} = \frac{\tau_{\mathrm{w}x}}{\mu} \quad (2a)$$

Inserting the Taylor expansion into the momentum equation and grouping by powers of y, we obtain the following expressions for the higher wall-normal de-

rivatives of the velocity profile at the wall:

$$\left.\frac{\partial^2 u}{\partial y^2}\right|_{\mathrm{w}} = \frac{1}{\mu}\left.\frac{\partial p}{\partial x}\right|_{\mathrm{w}} \tag{3a}$$

$$\left.\frac{\partial^3 u}{\partial y^3}\right|_{\mathrm{w}} = \frac{1}{\rho\nu^2}\frac{\partial \tau_{\mathrm{w}x}}{\partial t} - \frac{1}{\mu}\left(2\frac{\partial^2 \tau_{\mathrm{w}x}}{\partial x^2} + \frac{\partial^2 \tau_{\mathrm{w}z}}{\partial x\,\partial z}\right) \tag{3b}$$

The former relation is the trace of the wall-parallel momentum equation and represents the well known *compatibility condition at the wall* [12], whereas the latter relation (3b) is the trace of the y-derivative of the wall-parallel momentum equation and has been obtained by Dallmann and Gebing [10] in its two-dimensional form using the streamfunction.

As the pressure gradient at the wall is generally unknown, it must be extrapolated from the field. A Taylor expansion of the pressure in wall-normal direction gives

$$\frac{\partial p}{\partial x} = \left.\frac{\partial p}{\partial x}\right|_{\mathrm{w}} + \left(\frac{\partial^2 \tau_{\mathrm{w}x}}{\partial x^2} + \frac{\partial^2 \tau_{\mathrm{w}z}}{\partial x\,\partial z}\right) y + O(y^2) \tag{4}$$

where the wall-normal momentum and the continuity equation were used. As the pressure gradient is multiplied with y^2 in the Taylor expansion of the velocity, the overall approximation error of the velocity remains of order $O(y^4)$.

Please note that similar expressions can be obtained for the w-component by interchanging x and z, u and w, and $\tau_{\mathrm{w}x}$ and $\tau_{\mathrm{w}z}$. These have been omitted for the sake of brevity.

2.2. Compatibility conditions from the boundary layer equations

For high Reynolds number flow, we can apply the simplifications of boundary layer theory. We can neglect the wall-parallel derivatives in the viscous term as well as the wall-normal variation of the pressure. Based on these assumptions, we obtain the modified relations

$$\left.\frac{\partial^3 u}{\partial y^3}\right|_{\mathrm{w}} = \frac{1}{\rho\nu^2}\frac{\partial \tau_{\mathrm{w}x}}{\partial t} \tag{5}$$

for the third derivative of the velocity and

$$\frac{\partial p}{\partial x} = \left.\frac{\partial p}{\partial x}\right|_{\mathrm{w}} \tag{6}$$

for the pressure gradient.

2.3. Closure of the wall model

In order to close the equation, we neglect the $O(y^4)$ terms in equation (1) and impose a collocation condition at position y_{p}: $u(y_{\mathrm{p}}) = u_{\mathrm{p}}$. We obtain a differential equation for the wall shear stress:

$$\frac{\partial \tau_{\mathrm{w}x}}{\partial t} = -\frac{6\nu}{y_{\mathrm{p}}^2}\tau_{\mathrm{w}x} + \frac{6\rho\nu^2}{y_{\mathrm{p}}^3}(u_{\mathrm{p}} - u_{\mathrm{w}}) - \frac{3\nu}{y_{\mathrm{p}}}\left.\frac{\partial p}{\partial x}\right|_{\mathrm{p}} \tag{7}$$

As a consequence of the boundary layer assumptions, the equation is local and does not contain wall-parallel derivatives of the wall shear stress. This simplifies the implementation of the model considerably.

Instead of a collocation condition, a cell average value could be imposed to close the wall model [6]. Depending on the properties of the numerical scheme of the flow solver, this approach could be advantageous.

2.4. Discussion

The cubic wall model (7) forms part of a hierarchy of Taylor polynomial approximations starting with the linear and quadratic approximations

$$\tau_{\mathrm{w}x} = \frac{\mu}{y_{\mathrm{p}}}(u_{\mathrm{p}} - u_{\mathrm{w}}) \tag{8}$$

$$\tau_{\mathrm{w}x} = \frac{\mu}{y_{\mathrm{p}}}(u_{\mathrm{p}} - u_{\mathrm{w}}) - \frac{y_{\mathrm{p}}}{2}\left.\frac{\partial p}{\partial x}\right|_{\mathrm{p}} \tag{9}$$

with the latter suggested by [13]. Equation (9) is included in (7) as the steady state solution. Models of higher order can be derived by determining more terms in the Taylor expansions of velocity and pressure. These models feature a quadratic nonlinearity of the wall shear stress and an elliptic equation along the wall that determines the curvature of the pressure profile.

We see the main application of our model in the simulation of complex wall bounded flows for which the assumption of a classical turbulent boundary layer does not hold. An example for this is the flow around a wall-mounted cylinder where the wall shear stress follows a laminar boundary layer scaling [8]. However, since the wall model is based on a cubic polynomial, we expect that the model derived from the Navier-Stokes equations could be also applied as a wall boundary condition for high-order finite difference and finite volume codes.

In the computation of turbulent flow, an advantage of the proposed methodology is that the wall model is formulated in terms of the instantaneous wall shear stress. Consequently, the deficiency of the wall function approach that the instantaneous velocity profile is assumed to be of the same form as the mean velocity profile, is avoided. As the cubic wall model is derived solely from the pressure and viscous terms, the interpolation point y_{p} is constrained to lie in the viscous sublayer. This could be alleviated by using a higher order polynomial and by including a sub-grid scale model (e.g. the WALE model [14]) into the derivation of the compatibility conditions.

Using a variation of constants formula, it can be shown that the cubic contribution of the wall model results in a smoothing of the quadratic model (9):

$$\tau_{\mathrm{w}x} = \int_0^t \frac{6\nu}{y_{\mathrm{p}}^2} e^{-\frac{6\nu(t-t')}{y_{\mathrm{p}}^2}} \left(\frac{\mu}{y_{\mathrm{p}}}(u_{\mathrm{p}} - u_{\mathrm{w}}) - \frac{y_{\mathrm{p}}}{2}\left.\frac{\partial p}{\partial x}\right|_{\mathrm{p}}\right) \mathrm{d}t' + \tau_{\mathrm{w}x}|_{t=0}\, e^{-\frac{6\nu t}{y_{\mathrm{p}}^2}} \tag{10}$$

Consequently, the wall model has an exponentially decaying memory. The wall shear stress follows velocity and pressure fluctuations with a frequency below $6\nu/y_{\mathrm{p}}^2$, whereas higher frequencies are damped.

3. ANALYTICAL VALIDATION

In this section, we assess the accuracy of the wall model (7) when the exact velocity and pressure fields are assumed to be known. The difference between the modeled and the exact wall shear stress is expanded into a Taylor series in terms of the distance of the interpolation point y_p. For comparison, we also assess the accuracy of using linear and quadratic wall functions.

3.1. Stokes boundary layer

As a first test case, we choose the oscillatory Stokes boundary layer. It is an analytical solution of the Navier-Stokes equations in a semi-infinite domain bounded by a wall oscillating harmonically in its tangent plane. We consider the flow in the coordinate frame moving with the wall which leads to the appearance of an oscillatory pressure gradient $\underline{\nabla} p = -\rho\, U_0\, \sin(\Omega t)\, \underline{e}_x$. After the transient has decayed, the solution results as

$$u(t,y) = U_0 \left[e^{-\eta_\mathrm{s}} \cos\left(\Omega t - \eta_\mathrm{s}\right) - \cos\left(\Omega t\right) \right] \tag{11}$$

with the normalised coordinate $\eta_\mathrm{s} = y/\delta_\mathrm{s}$ and the boundary layer thickness $\delta_\mathrm{s} = \sqrt{2\nu/\Omega}$ [12]. The wall shear stress can be obtained as

$$\tau_{\mathrm{w}x} = \mu \sqrt{\frac{\Omega}{\nu}} U_0 \sin\!\left(\Omega t - \frac{\pi}{4}\right) \tag{12}$$

and it advances the outer flow by a quarter of a period.

We evaluate the linear, quadratic and cubic model for the velocity field (11) and perform a Taylor series expansion in y_p. For the linear model (8), we obtain

$$\tau_{\mathrm{w}x,\mathrm{lin}} - \tau_{\mathrm{w}x} = -\frac{\rho \Omega U_0}{2} \sin(\Omega t)\, y_\mathrm{p} + O(y_\mathrm{p}^2)\,, \tag{13}$$

for the quadratic model (9), we obtain

$$\begin{aligned} \tau_{\mathrm{w}x,\mathrm{quad}} - \tau_{\mathrm{w}x} = -\frac{\rho \Omega U_0}{6} \sqrt{\frac{\Omega}{\nu}} \sin\!\left(\Omega t + \frac{\pi}{4}\right) y_\mathrm{p}^2 \\ + O(y_\mathrm{p}^3)\,, \end{aligned} \tag{14}$$

and for the cubic model (7), we obtain

$$\tau_{\mathrm{w}x,\mathrm{cub}} - \tau_{\mathrm{w}x} = -\frac{\rho \Omega^2 U_0}{24\,\nu} \cos(\Omega t)\, y_\mathrm{p}^3 + O(y_\mathrm{p}^4)\,. \tag{15}$$

The a-priori value of the wall shear stress from the cubic wall model is therefore third-order accurate in the wall distance of the interpolation point y_p.

3.2. Falkner-Skan boundary layer

The Falkner-Skan boundary layer [12] is a self-similar solution to the laminar boundary layer equations for flow around a wedge. The solution is characterised by the parameter β; the interior angle of the wedge is given as $\beta\pi$. For $\beta = 0$ and $\beta = 1$, the Falkner-Skan solution corresponds to the Blasius boundary layer and the plane stagnation point flow, respectively.

The solution to the Falkner-Skan boundary layer is given as

$$u(x,y) = U(x) f'(\eta) \tag{16}$$

with the similarity variable

$$\eta = y \sqrt{\frac{1}{2-\beta} \frac{U(x)}{\nu x}}\,. \tag{17}$$

The dimensionless stream function $f(\eta)$ satisfies the differential equation

$$f''' + f f'' + \beta(1 - f'^2) = 0 \tag{18}$$

with $f(0) = 0$, $f'(0) = 0$ and $f'(\infty) = 1$. The exact wall shear stress is given as

$$\tau_{\mathrm{w}x} = \mu U(x) \sqrt{\frac{1}{(2-\beta)} \frac{U(x)}{\nu x}}\, f''_\mathrm{w} \tag{19}$$

where $f''_\mathrm{w} = f''(0)$ is solely a function of β.

We evaluate the linear and quadratic wall function as well as the steady state of the wall model (7) and perform a Taylor expansion. For the linear wall function, the error results as

$$\tau_{\mathrm{w}x,\mathrm{lin}} - \tau_{\mathrm{w}x} = -\frac{\beta}{2-\beta} \frac{\rho U(x)^2}{2x}\, y_\mathrm{p} + O(y_\mathrm{p}^2) \tag{20}$$

which is first-order accurate in the distance of the interpolation point y_p. For the quadratic wall function as well as for the cubic wall model, we obtain

$$\begin{aligned} \tau_{\mathrm{w}x,\mathrm{quad}} - \tau_{\mathrm{w}x} &= \tau_{\mathrm{w}x,\mathrm{cub}} - \tau_{\mathrm{w}x} \\ &= \frac{2\beta - 1}{(2-\beta)^2} f''^2_\mathrm{w} \frac{\rho U(x)^3}{24 \nu x^2}\, {y_\mathrm{p}}^3 + O(y_\mathrm{p}^4)\,. \end{aligned} \tag{21}$$

The a-priori value of the wall shear stress of the cubic wall model is again third-order accurate in y_p. As the flow is steady, the time derivative of the wall shear stress is zero and the predictions of the quadratic and cubic model are the same.

4. NUMERICAL VALIDATION

In this section, we investigate the accuracy of the wall model (7) when the velocity field is unknown and the evaluation of the wall model is coupled to the direct numerical simulation or large-eddy simulation of the velocity and pressure fields. This approach permits to assess feedback effects between the wall model and the flow solution. We compare the predictive performance of the linear approximation (8) and our model (7) depending on the grid resolution.

4.1. Description of the flow solver

The simulations were performed using our in-house code MGLET [15]. It uses a second-order central finite volume scheme on a block-structured Cartesian grid with a staggered arrangement of variables [16]. The time integration employs a third-order low-storage explicit Runge-Kutta scheme [17] and the divergence-free constraint of the velocity field is enforced in every substep by solving a Poisson equation for a correction pressure [18].

Flow in complex geometries is treated using

a cut-cell immersed boundary method based on [19, 20]. This discretisation preserves the skew-symmetry of the convective term and the positive-definiteness of the diffusive term. The time step restriction due to the small cells that occur invariably as a complex geometry intersects a Cartesian grid is circumvented with a merging strategy.

4.2. Implementation details

In the following, we comment on some noteworthy aspects of the coupling of the wall model into our flow solver. The wall shear stress appears explicitly as a momentum flux in the finite volume balance of the cut-cells. For each cut-cell, the velocity vector and pressure gradient are interpolated to a point at a wall-normal distance of $y_\mathrm{p} = \Delta y$ and the wall-normal component is removed from both vectors [21]. Then, either the linear wall function (8) or our wall model is used to compute the wall shear stress vector from the tangential velocity and pressure gradient. Please note that the linear wall function is the default second-order approximation of the diffusive term [21]. We use a vectorial form of the wall model (7) derived from the boundary layer equations:

$$\begin{aligned}\frac{\partial \underline{\tau}_\mathrm{w}}{\partial t} = &-\frac{6\nu}{y_\mathrm{p}^2}\underline{\tau}_\mathrm{w} + \frac{6\rho\nu^2}{y_\mathrm{p}^3}\left[\underline{\underline{I}} - \underline{n}\otimes\underline{n}\right](\underline{u}_\mathrm{p} - \underline{u}_\mathrm{w}) \\ &-\frac{3\nu}{y_\mathrm{p}}\left[\underline{\underline{I}} - \underline{n}\otimes\underline{n}\right]\nabla p\big|_\mathrm{p}\end{aligned} \tag{22}$$

We integrate this equation using the same explicit Runge-Kutta scheme as for the momentum equation. The coupling is implemented by simply updating the values at the beginning of each stage of the Runge-Kutta scheme.

For the present choice of the wall distance y_p of the interpolation point the stability of the time integration scheme is not affected. In particular, the critical ratio $6\nu\Delta t/y_\mathrm{p}^2 = 6\nu\Delta t/\Delta x^2$ that can be obtained from the decay constant of the wall model is equal to the diffusion number of a cubic open fluid cell.

4.3. Stokes boundary layer

We simulated the oscillatory Stokes boundary layer flow (11) on a domain $[0, 31\,\delta_\mathrm{s}]$. A no-slip boundary condition is applied at the bottom and a slip boundary condition is applied at the top. We use a cell size of $0.05\,\delta_\mathrm{s}$, $0.1\,\delta_\mathrm{s}$, …, $3.2\,\delta_\mathrm{s}$. The flow was started from rest and the calculation was performed until $\Omega t = 50$. Due to the slow decay of the transient and our explicit time integration scheme, it was not economical to simulate the flow until a steady oscillation was reached. Instead, we compare the solution to the analytical solution of [22] for the transient flow in response to a sinusoidal pressure gradient.

Fig. 1 shows the convergence of the velocity field $u(y,t)$ to the analytical solution in the L^2 norm computed over space and time. The velocity is interpolated linearly between the grid points. We observe a second order convergence of the solution for both the linear wall function (as expected) and the cubic wall

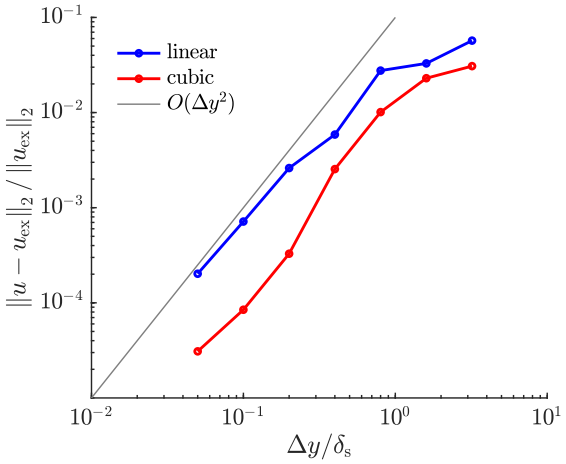

Figure 1. Convergence of the velocity field $u(y,t)$ for the transient Stokes boundary layer in the space-time L^2-norm.

model. The error for the cubic wall model (22) is approximately a third to half of the error for the linear wall function. Notably, the cubic wall model maintains an advantage over the linear wall function also for very coarse grids. For the same error, the wall model allows to coarsen the grid by a factor of 2.

4.4. Plane stagnation point flow

In this section, we investigate the accuracy of the wall model for the plane stagnation point flow (a Falkner-Skan boundary layer with $\beta = 1$) which is an exact semi-analytic solution of the Navier-Stokes equations [12]. This flow has the property that the boundary layer thickness is constant in space. This allows us to choose a constant grid resolution of the boundary layer. Furthermore, the plane stagnation point flow is prototypical for stagnation points that appear in flow around bluff bodies. As the boundary layer is often thinnest at the stagnation point, the resolution of this flow can dictate the overall grid resolution requirements.

The flow was simulated in a rectangular domain of height $12\sqrt{\nu/a}$ and width $36\sqrt{\nu/a}$. At the top of the domain, we applied a constant inflow velocity $v = -ay$ with a Neumann boundary condition for the velocity u. At the left ($x = 0$), we apply a symmetry boundary condition. At the bottom ($y = 0$), we apply the wall shear stress from the wall function or wall model. At the right, we assign a constant pressure $p = 0$ (this is inconsistent with the analytical solution). We varied the cell size in powers of 2 from $\Delta y/\delta_{99} = 0.0161$ to 0.514. At the coarsest grid resolution, the boundary layer is therefore contained in only two cells.

The corresponding analytical solution is derived from the potential flow with $u = \tilde{a}x$ and $v = -\tilde{a}y$ and

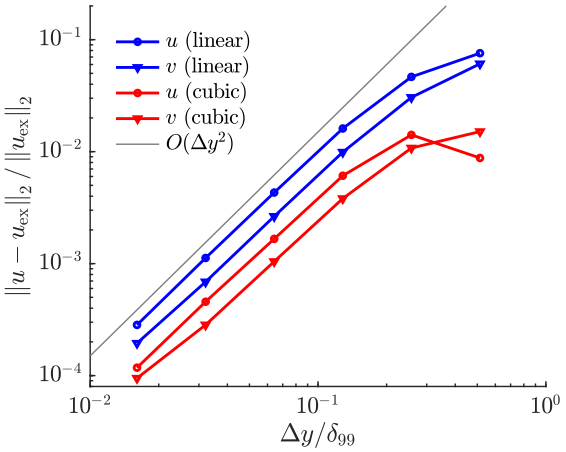

Figure 2. Convergence of the velocity profiles $u(y)$ and $v(y)$ at $x = \sqrt{\nu/\tilde{a}}$ for the plane stagnation point flow in the L^2-norm computed over the y-direction.

has the form

$$u(x, y) = \tilde{a} x f'(\eta) \tag{23a}$$

$$v(x, y) = -\sqrt{\tilde{a}\nu}\, f(\eta) \tag{23b}$$

where the dimensionless stream function $f(\eta)$ is a solution to the Falkner-Skan equation (18) for $\beta = 1$. Due to the displacement effect of the boundary layer, the constant $\tilde{a}$ must be chosen differently from the value a in the simulation. We set a value $\tilde{a} = 1.0556\, a$ that is derived from the requirement that the analytical solution matches the inflow profile of the simulation. In particular, the constant $\tilde{a}$ is a solution to

$$\sqrt{\tilde{a}/a}\, f\left(12\sqrt{\tilde{a}/a}\right) = 12 \tag{24}$$

Fig. 2 shows the convergence of the velocity profiles at $x = \sqrt{\nu/\tilde{a}}$ in the L^2-norm computed over the y-coordinate. It is apparent that the wall model significantly improves the prediction of the velocity field. In particular, at the coarsest grid resolution the cubic wall model is approximately as accurate as the linear wall function with a grid refined by a factor of 4.

4.5. Turbulent channel flow

In order to verify the correctness and robustness of the wall model (22) and to establish resolution requirements in turbulent flow, we performed LES of turbulent flow in a plane channel at a Reynolds number $Re_\tau = \frac{u_\tau h}{\nu} = 180$ with the friction velocity $u_\tau = \sqrt{\tau_w/\rho}$ and the half-height h. As reference data we use the direct numerical simulation (DNS) of [23]. The length of the domain is chosen like in [24] as $4\pi h$ in streamwise (x) and $2\pi h$ in spanwise (z) direction and the y-coordinate goes from $-h$ to h. The flow is driven by a constant pressure gradient. The sub-grid stresses are modelled with the WALE-viscosity model of Nicoud and Ducros [14].

We consider three grid resolutions for which the viscous sublayer is marginally resolved. At the coarsest resolution, the grid has a uniform cell size of $\Delta x^+ = \frac{u_\tau \Delta x}{\nu} = 24$ wall units in the streamwise, $\Delta y^+ = 6$ wall units in the wall-normal and $\Delta z^+ = 12$ wall units in the spanwise directions. At the intermediate resolution, the grid has a cell size of $\Delta x^+ = 18$, $\Delta y^+ = 4.5$ and $\Delta z^+ = 9$ wall units and at the finest resolution, the cell sizes are $\Delta x^+ = 12$, $\Delta y^+ = 3$ and $\Delta z^+ = 6$ wall units. Consequently, the interpolation point that is used to compute the wall shear stress lies at a distance of $y_p^+ = 6$, $y_p^+ = 4.5$ and $y_p^+ = 3$ wall units, respectively. Flow statistics were collected over approximately 50 flow-through times and further averaged over the x- and z-direction.

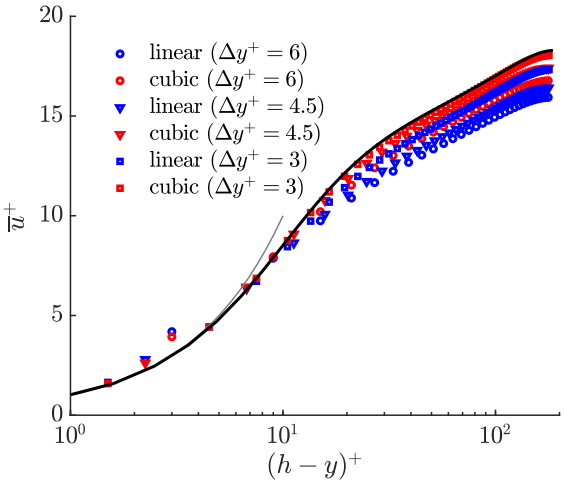

Figure 3. Mean velocity profile inside the turbulent channel flow for $Re_\tau = 180$. The symbols represent the velocity profiles obtained from our LES, the black line represents the DNS by Hoyas and Jiménez [23]. The grey line displays the linear law of the wall $u^+ = y^+$.

Fig. 3 shows the profile of the mean streamwise velocity $\overline{u}$ normalised with wall units (i.e. ν and u_τ) over the wall distance. We can see that the simulation results with the wall model show a significant improvement over the results computed with the linear law of the wall. For example, the results of the wall model at $\Delta y^+ = 4.5$ (red triangles) are approximately identical to the results obtained with the linear wall function at $\Delta y^+ = 3$ (blue squares). Furthermore, the results from the wall model at y_p^+ lie very close to the DNS reference. Please note that the wall shear stress is computed by interpolating the velocity to y_p – in the present grid configuration that means taking the average value between the two velocities closest to the wall – and then imposing either the linear wall function (indicated by the dotted line) or feeding the value into the wall model. Therefore, the velocity closest to the wall overshoots the linear law of the wall at the coarse grid resolution.

Fig. 4 shows the profile of the Reynolds shear stress $-\overline{u'v'}$ normalised with wall units (i.e. ν and

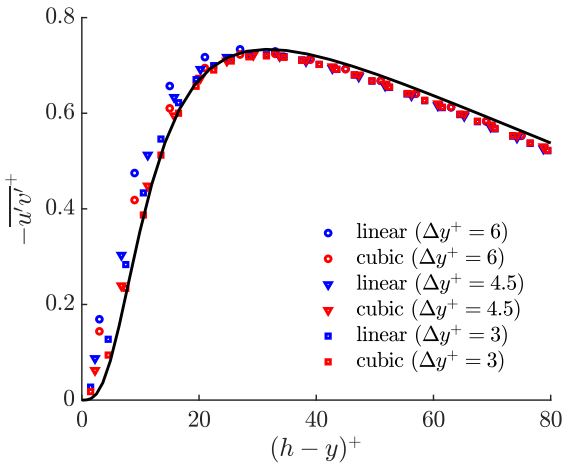

Figure 4. Reynolds shear stress profile inside the turbulent channel flow for $Re_\tau = 180$. The symbols represent the velocity profiles obtained from our LES, the black line represents the DNS by Hoyas and Jiménez [23].

u_τ) over the wall distance. Again, the wall model exhibits a marked improvement over the linear law of the wall particularly in the buffer layer.

It follows from the near-wall behaviour of the velocity that at leading order in the wall distance $h - y$ the Reynolds shear stress only depends on the wall shear stress fluctuation field (cf. Smits et al. [25]):

$$-\overline{u'v'} \approx \frac{1}{2\mu^2}\overline{\tau'_{wx}\left(\frac{\partial \tau'_{wx}}{\partial x} + \frac{\partial \tau'_{wz}}{\partial z}\right)}(h-y)^3 \qquad (25)$$

Therefore, the improved prediction of the Reynolds shear stress near the wall directly reflects a better prediction of the wall shear stress fluctuations.

The improvement in the mean velocity profile is mainly attributed to the inclusion of the pressure gradient which at this relatively low Reynolds number dominates the near wall part of the buffer layer. The more accurate Reynolds shear stress further improves the prediction.

For higher Reynolds numbers, the contribution of the pressure gradient to the mean velocity profile decreases with $1/Re_\tau$ [26]. In light of the findings of Smits et al. [25], we expect that including the time derivative of the wall shear stress into the wall model remains important also for high Reynolds numbers.

5. CONCLUSION

A wall model was derived based on a cubic Taylor polynomial for the velocity profile and a linear profile for the pressure. The wall-normal velocity derivatives were expressed in terms of the wall shear stress and the wall pressure using relations obtained from the Navier-Stokes [10] or boundary layer equations. By imposing a collocation constraint for the velocity at a point off the wall, we obtained an ordinary differential equation for the wall shear stress.

We first conducted an a-priori investigation in which the wall shear stress was computed from a known velocity profile. For the oscillatory Stokes boundary layer and the Falkner-Skan boundary layer, we found that our wall model converges to the exact wall shear at third order in the distance of the interpolation point. We observed that for small distances from the wall, the model has a superior accuracy than a linear approximation when a pressure gradient is present and a superior accuracy than both a linear and a quadratic approximation [13] when the flow is unsteady.

In a second step, we performed a-posteriori tests for which the wall model was coupled to a flow solver. For the same test cases, we observed that the wall model achieves the same accuracy as the linear wall function for half the grid resolution. Use of the wall model resulted in reasonably accurate solutions when there are two or more cells over the 99% boundary layer thickness. Finally, we performed wall-resolved LES of a turbulent channel flow at $Re_\tau = 180$ at various grid resolutions for which the interpolation point lies within the viscous sublayer. We found that the wall model achieves the same accuracy as the linear wall function for two thirds of the grid resolution.

In conclusion, the present wall model can deliver significant gains in accuracy at the same grid resolution (or significant savings in grid points at the same accuracy) for LES that marginally resolve boundary layers or the viscous sublayer in turbulent flow.

Future work might combine the present model with the model of Breuer et al. [6] by replacing their quadratic approximation of the velocity profile within the viscous sublayer with the cubic approximation derived in sections 2.1–2.3. It could also be interesting to investigate other velocity profiles than the Taylor polynomials. As already noted by [11], the monomial basis could be replaced by a different function basis with a higher approximation power, e.g. rational functions.

ACKNOWLEDGEMENTS

The authors gratefully acknowledge the computational and data resources provided by the Leibniz Supercomputing Centre (`www.lrz.de`).

REFERENCES

[1] Shih, T.-H., Povinelli, A., Liu, N.-S., Potapczuk, G., and Lumley, J. L., 1999, "A Generalized Wall Function", *Technical Memorandum 19990081113*, NASA.

[2] Balaras, E., and Benocci, C., 1994, "Subgrid Scale Models in Finite Difference Simulations of Complex Wall Bounded Flows", *Applications of Direct and Large Eddy Simulation, AGARD*, Chania, Greece, Vol. 551, pp. 2.1–2.6.

[3] Cabot, W., and Moin, P., 2000, "Approximate Wall Boundary Conditions in the Large-Eddy Simulation of High Reynolds Number Flow",

Flow, Turbulence and Combustion, Vol. 63 (1), pp. 269–291.

[4] Spalart, P., Jou, W.-H., Strelets, M., and Allmaras, S., 1997, "Comments on the Feasibility of LES for Wings, and on a Hybrid RANS/LES Approach", *Proceedings of First AFOSR International Conference on DNS/LES*, Greyden Press.

[5] Werner, H., and Wengle, H., 1993, "Large-eddy simulation of turbulent flow over and around a cube in a plate channel", F. e. a. Durst (ed.), *Turbulent Shear Flows 8*, Springer, Berlin, pp. 155–168.

[6] Breuer, M., Kniazev, B., and Abel, M., 2007, "Development of Wall Models for LES of Separated Flows Using Statistical Evaluations", *Computers & Fluids*, Vol. 36 (5), pp. 817–837.

[7] Schanderl, W., Jenssen, U., and Manhart, M., 2017, "Near-Wall Stress Balance in Front of a Wall-Mounted Cylinder", *Flow, Turbulence and Combustion*, Vol. 99, pp. 665–684.

[8] Jenssen, U., Schanderl, W., Strobl, C., Unglehrt, L., and Manhart, M., 2021, "The Viscous Sublayer in Front of a Wall-Mounted Cylinder", *Journal of Fluid Mechanics*, Vol. 919, p. A37.

[9] Schanderl, W., and Manhart, M., 2016, "Reliability of wall shear stress estimations of the flow around a wall-mounted cylinder", *Computers and Fluids*, Vol. 128, pp. 16–29.

[10] Dallmann, U., and Gebing, H., 1994, "Flow Attachment at Flow Separation Lines", G. H. Schnerr, R. Bohning, W. Frank, and K. Bühler (eds.), *Fluid- and Gasdynamics*, Acta Mechanica, Springer, Vienna, ISBN 978-3-7091-9310-5, pp. 47–56.

[11] Shrikhande, G., 2012, "Assessment of Taylor-series Model for Estimation of Vortex Flows Using Surface Stress Measurements", Master's thesis, Michigan State University.

[12] Schlichting, H., and Gersten, K., 2006, *Grenzschicht-Theorie*, Springer, Berlin Heidelberg, ISBN 978-3-540-23004-5.

[13] Manhart, M., Peller, N., and Brun, C., 2008, "Near-Wall Scaling for Turbulent Boundary Layers with Adverse Pressure Gradient", *Theoretical and Computational Fluid Dynamics*, Vol. 22 (3), pp. 243–260.

[14] Nicoud, F., and Ducros, F., 1999, "Subgrid-Scale Stress Modelling Based on the Square of the Velocity Gradient Tensor", *Flow, Turbulence and Combustion*, Vol. 62 (3), pp. 183–200.

[15] Manhart, M., Tremblay, F., and Friedrich, R., 2001, "MGLET: A Parallel Code for Efficient DNS and LES of Complex Geometries", *Parallel Computational Fluid Dynamics 2000*, North-Holland, Amsterdam, ISBN 978-0-444-50673-3, pp. 449–456.

[16] Harlow, F. H., and Welch, J. E., 1965, "Numerical Calculation of Time-Dependent Viscous Incompressible Flow of Fluid with Free Surface", *The Physics of Fluids*, Vol. 8 (12), pp. 2182–2189.

[17] Williamson, J., 1980, "Low-Storage Runge-Kutta Schemes", *Journal of Computational Physics*, Vol. 35 (1), pp. 48–56.

[18] Chorin, A. J., 1968, "Numerical Solution of the Navier-Stokes Equations", *Mathematics of Computation*, Vol. 22 (104), pp. 745–762.

[19] Dröge, M., and Verstappen, R., 2005, "A New Symmetry-Preserving Cartesian-Grid Method for Computing Flow Past Arbitrarily Shaped Objects", *International Journal for Numerical Methods in Fluids*, Vol. 47 (8-9), pp. 979–985.

[20] Cheny, Y., and Botella, O., 2010, "The LS-STAG Method: A New Immersed Boundary/Level-Set Method for the Computation of Incompressible Viscous Flows in Complex Moving Geometries with Good Conservation Properties", *Journal of Computational Physics*, Vol. 229 (4), pp. 1043–1076.

[21] Meyer, M., Devesa, A., Hickel, S., Hu, X. Y., and Adams, N. A., 2010, "A Conservative Immersed Interface Method for Large-Eddy Simulation of Incompressible Flows", *Journal of Computational Physics*, Vol. 229 (18), pp. 6300–6317.

[22] Liu, C.-M., and Liu, I.-C., 2006, "A Note on the Transient Solution of Stokes' Second Problem with Arbitrary Initial Phase", *Journal of Mechanics*, Vol. 22 (4), pp. 349–354.

[23] Hoyas, S., and Jiménez, J., 2006, "Scaling of the Velocity Fluctuations in Turbulent Channels up to Reτ=2003", *Physics of Fluids*, Vol. 18 (1), p. 011702.

[24] Kim, J., Moin, P., and Moser, R., 1987, "Turbulence Statistics in Fully Developed Channel Flow at Low Reynolds Number", *Journal of Fluid Mechanics*, Vol. 177, pp. 133–166.

[25] Smits, A. J., Hultmark, M., Lee, M., Pirozzoli, S., and Wu, X., 2021, "Reynolds Stress Scaling in the Near-Wall Region of Wall-Bounded Flows", *Journal of Fluid Mechanics*, Vol. 926.

[26] Pope, S. B., 2000, *Turbulent Flows*, Cambridge University Press, Cambridge; New York, ISBN 978-0-521-59125-6 978-0-521-59886-6.